PROCEEDINGS OF SCIENCE

Sparse modeling study to extract spectral functions from lattice QCD data

Junichi Takahashi,[a,*] **Hiroshi Ohno**[b] **and Akio Tomiya**[c]

[a] *Meteorological College, Japan Meteorological Agency,*
7-4-81, Asahi-cho, Kashiwa, Chiba 277-0852, Japan
[b] *Center for Computational Sciences, University of Tsukuba,*
1-1-1, Tennodai, Tsukuba, Ibaraki 305-8577, Japan
[c] *Department of Information and Mathematical Sciences, Tokyo Woman's Christian University,*
2-6-1, Zempukuji, Suginami-ku, Tokyo 167-8585, Japan
E-mail: mhjkk-takahashi@met.kishou.go.jp, hohno@ccs.tsukuba.ac.jp, akio@yukawa.kyoto-u.ac.jp

We present spectral functions extracted from Euclidean-time correlation functions by using sparse modeling. Sparse modeling is a method that solves inverse problems by considering only the sparseness of the solution we seek. To check applicability of the method, we firstly test it with mock data which imitate charmonium correlation functions on a fine lattice. We show that the method can reconstruct the resonance peaks in the spectral functions. Then, we extract charmonium spectral functions from correlation functions obtained from lattice QCD at temperatures below and above the critical temperature T_c. We show that this method yields results like those obtained with MEM and other methods.

The 41st International Symposium on Lattice Field Theory (LATTICE2024)
28 July - 3 August 2024
Liverpool, UK

*Speaker

PoS(LATTICE2024)032

1. Introduction

Theoretically accessible real-frequency spectral functions are crucial for the study of properties of the hot and dense medium such as the Quark-Gluon Plasma [1–4]. However, the extraction of these spectral functions presents a significant challenge due to the inability to obtain them directly from lattice QCD calculations.

In lattice QCD, an imaginary time description is employed to calculate the correlation function G of Euclidean time τ, which relates the spectral function ρ of frequency ω through the following integral equation:

$$G(\tau) = \int_0^\infty d\omega K(\omega, \tau)\rho(\omega), \tag{1}$$

where K is the integration kernel defined by

$$K(\omega, \tau) \equiv \frac{\cosh\left[\omega\left(\tau - \frac{1}{2T}\right)\right]}{\sinh\left(\frac{\omega}{2T}\right)} \tag{2}$$

in the Euclidean time range $0 \leq \tau \leq 1/T$ with temperature T. Consequently, in order to obtain spectral functions, it is necessary to perform analytical continuations from correlation functions. In general, the correlation functions obtained by lattice QCD contain noise, and the analytical continuation is extremely sensitive to this noise.

When the frequency ω is discretized, eq. (1) can be simply written as a linear equation

$$\vec{G} = K\vec{\rho}, \tag{3}$$

where $\vec{G}$ and $\vec{\rho}$ are M and N dimensional vectors, respectively, and K is an $M \times N$ matrix. For typical lattice QCD calculations the temporal lattice size, i.e., M is of $O(10)$ while N must be of $O(10^3)$ for sufficiently good resolution of the spectral function. Therefore, solving eq. (3) to extract the spectral function is an ill-posed inverse problem.

There have been lots of previous studies on extracting spectral functions from lattice QCD data, employing a variety of techniques based on different ideas [5–7]. Sparse modeling is one of such techniques, which was recently applied for the first time to lattice QCD data to obtain spectral functions of the energy-momentum tensor and the shear viscosity [8]. In Ref. [9], we have considered the covariance between different Euclidean times of the correlation function when utilizing sparse modeling, checked the applicability of the method and extracted the charmonium spectral functions. In this study we aim to conduct a more comprehensive investigation into the applicability of sparse modeling. Furthermore, we also compare our results with those of one of the previous studies to properly estimate the systematic uncertainty.

2. Sparse modeling

Extracting spectral functions by using sparse modeling has been proposed in condensed matter physics [10, 11] (see also a review paper [12] for detail). The procedure of the sparse modeling is outlined in Ref. [9], and we summarize the key characteristics of the sparse modeling in the following three points.

First, the reduction in rank of the spectral functions and correlation functions is achieved by the exclusion of the contribution of small singular values after their bases are transformed as follows,

$$\vec{G}' \equiv U^{\mathrm{t}}\vec{G}, \quad \vec{\rho}^{\,\mathrm{t}} \equiv V^{\mathrm{t}}\vec{\rho}, \tag{4}$$

where U and V are $M \times M$ and $N \times N$ orthogonal matrices, respectively, obtained through the singular value decomposition of the kernel K,

$$K = USV^{\mathrm{t}}, \tag{5}$$

where S is a diagonal matrix composed of singular values. In this study, we retain only the components of $\vec{\rho}'$ and $\vec{G}'$ that fulfill the condition $s_l/s_1 \geq 10^{-15}$ where s_l is the l-th largest singular value. The number of components that satisfy this condition is denoted as L. Thus the rank of the retained components is L and the size of U, V and S become $M \times L$, $N \times L$ and $L \times L$, respectively.

Second, an L_1 regularization term is incorporated into the cost function based on the square error, making the optimization problem a form of Least Absolute Shrinkage and Selection Operator (LASSO). The cost function that we seek to minimise can be expressed as follows,

$$F(\vec{\rho}') = \frac{1}{2}(\vec{G}' - S\vec{\rho}')^2 + \lambda||\vec{\rho}'||_1, \tag{6}$$

where $||\cdot||_1$ stands for the L_1 norm defined by $||\vec{\rho}'||_1 \equiv \sum_{i=1}^{L} |\rho_i'|$ and λ is a positive hyperparameter which controls the contribution of the L_1 regularization relative to the square error. This regularization promotes sparsity in the solution of $\vec{\rho}'$.

Third, this optimization problem is solved iteratively by alternating direction method of multipliers (ADMM) algorithm [13]. In this study, the problem is solved for multiple values of λ, and the most likely spectral function $\vec{\rho}$ is determined at the optimal value λ_{opt}. The estimation of λ_{opt} follows the procedure used in previous work [8].

3. Mock data tests

Before we apply the sparse modeling to the actual lattice QCD data, we test it with mock data which imitate possible charmonium spectral functions.

Following in Ref. [6], we make the input spectral functions at temperatures below and above T_{c}:

- For $T < T_{\mathrm{c}}$,
  $\hat{\rho}_{\mathrm{below}}(\hat{\omega}) = \tilde{\Theta}(\hat{\omega}, \hat{\omega}_1, \Delta_1)(1 - \tilde{\Theta}(\hat{\omega}, \hat{\omega}_2, \Delta_2))\hat{\rho}_{\mathrm{res}} + \tilde{\Theta}(\hat{\omega}, \hat{\omega}_3, \Delta_3)\hat{\rho}_{\mathrm{Wilson}}$.
- For $T > T_{\mathrm{c}}$,
  $\hat{\rho}_{\mathrm{above}}(\hat{\omega}) = \hat{\rho}_{\mathrm{trans}} + \tilde{\Theta}(\hat{\omega}, \hat{\omega}_4, \Delta_4)(1 - \tilde{\Theta}(\hat{\omega}, \hat{\omega}_5, \Delta_5))\hat{\rho}_{\mathrm{res}} + \tilde{\Theta}(\hat{\omega}, \hat{\omega}_6, \Delta_6)\hat{\rho}_{\mathrm{Wilson}}$.

Here $\hat{\rho}_{\mathrm{res}}$, $\hat{\rho}_{\mathrm{trans}}$ and $\hat{\rho}_{\mathrm{Wilson}}$ denote a resonance peak, a transport peak and a free Wilson spectral function, respectively, and the hatted letters are dimensionless quantities. The function $\tilde{\Theta}$ is a modified Θ function introduced to smoothly connect each spectral function. In Ref. [6], free continuum spectral function is employed in $\hat{\rho}_{\mathrm{below}}$. In this study, however, free Wilson spectral

Spectral function	Parameters
$\hat{\rho}_{\rm res}$ for $\hat{\rho}_{\rm below}$	$c_{\rm res} = 0.08/7$, $\Gamma = 0.05$, $M = 0.155$
$\hat{\rho}_{\rm Wilson}$ for $\hat{\rho}_{\rm below}$	$c_{\rm Wilson} = 0.5$, $b^{(1)} = 2$, $b^{(2)} = 1$, $m = 0.073$, $N_c = 3$, $N_\sigma = 4096$
$\hat{\rho}_{\rm trans}$ for $\hat{\rho}_{\rm above}$	$c_{\rm trans} = 5 \times 10^{-5}$, $\eta = 0.006$
$\hat{\rho}_{\rm res}$ for $\hat{\rho}_{\rm above}$	$c_{\rm res} = 0.06$, $\Gamma = 0.15$, $M = 0.225$
$\hat{\rho}_{\rm Wilson}$ for $\hat{\rho}_{\rm above}$	$c_{\rm Wilson} = 1$, $b^{(1)} = 3$, $b^{(2)} = 1$, $m = 0.073$, $N_c = 3$, $N_\sigma = 4096$

Table 1: Parameters for the mock spectral functions. See Ref. [6] for notations.

function is utilized to account for lattice cutoff effects at temperature below $T_{\rm c}$. For details on the functional forms of $\hat{\rho}_{\rm res}$, $\hat{\rho}_{\rm trans}$, $\hat{\rho}_{\rm Wilson}$ and $\tilde{\Theta}$, see Ref. [6].

The values of the parameters used in the above spectral functions are summarized in table 1. The position of the resonance peak is about J/ψ meson mass (~ 3.1 GeV) for $T < T_{\rm c}$, and a transport peak appears and the resonance peak becomes broader for $T > T_{\rm c}$. The values of the parameters used in the modified Θ function are same as Ref. [6]. In this study, we consider that the range of frequencies $\hat{\omega}$ is from 0 to 4 with 8,001 points in $\hat{\omega}$-space.

The central values of correlation function $G(\tau)$ are given by integrating the input spectral function and the kernel. The kernel is given in eq. (2), which diverges at $\omega = 0$. Moreover, the correlation function is influenced by lattice cutoff effects at small τ distances. To address these issues, we used a modified kernel and a modified spectral function defined by

$$\tilde{K}(\hat{\omega}, \hat{\tau}; \hat{\tau}_0) \equiv \hat{\omega}\frac{K(\hat{\omega}, \hat{\tau})}{K(\hat{\omega}, \hat{\tau}_0)} = \hat{\omega}\frac{\cosh\left[\hat{\omega}\left(\hat{\tau} - \frac{N_\tau}{2}\right)\right]}{\cosh\left[\hat{\omega}\left(\hat{\tau}_0 - \frac{N_\tau}{2}\right)\right]}, \quad \tilde{\rho}(\hat{\omega}; \hat{\tau}_0) = \frac{\hat{\rho}(\hat{\omega})}{\hat{\omega}}K(\hat{\omega}, \hat{\tau}_0), \tag{7}$$

and we used the mock correlation function data from $\hat{\tau}_0$ to $N_\tau/2$, where $\hat{\tau}_0$ was set to 1 in our mock data tests. Errors of $G(\tau)$ are generated by gaussian random numbers with the variance $\sigma(\tau) = \varepsilon \cdot \tau \cdot G(\tau)$ in order to incorporate the fact that the error of lattice correlation functions increases as τ increases. One of the purpose of this study is to examine the applicability of sparse modeling to the number of input data and the magnitude of noise. Therefore, we consider three types of temporal extents, $N_\tau = 48$, 64 and 96, and three types of noise levels, $\varepsilon = 10^{-2}$, 5×10^{-3} and 10^{-5} in our mock data tests.

Figure 1 shows the spectral functions as a function of $\hat{\omega}$ for $T < T_{\rm c}$. In Fig. 1(a), the results with a fixed noise level of $\varepsilon = 5 \times 10^{-3}$ for various N_τ are illustrated. The blue solid line represents the input spectral function, and the black dashed, green dotted and red dash-dotted lines represent the output results with $N_\tau = 48$, 64 and 96, respectively. Increasing N_τ results in better spectral functions that are closer to the input spectral function. Similar results are obtained for the other noise levels ε. In Fig. 1(b), the results with a fixed temporal extent of $N_\tau = 96$ for various ε are illustrated. The black dashed, green dotted and red dash-dotted lines represent the output results with $\varepsilon = 10^{-2}$, 5×10^{-3} and 10^{-5}, respectively. The meaning of the blue solid line is same as Fig. 1(a). Reducing ε results in better spectral functions that are closer to the input spectral function. Similar results are obtained for the other temporal extents N_τ.

Same results as Fig. 1 but for $T < T_{\rm c}$ are shown in Fig. 2, where $\varepsilon = 10^{-2}$ and $N_\tau = 48$ are chosen in Fig. 2(a) and Fig. 2(b), respectively. ε and N_τ dependences are also the same as Fig. 1,

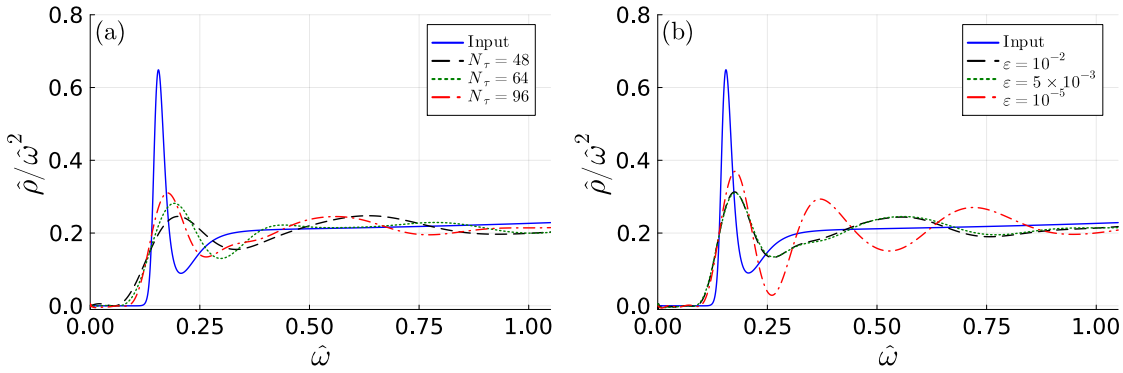

Figure 1: Spectral functions calculated by using sparse modeling in the mock-data tests for $T < T_c$. Figure (a) shows the results with a fixed noise level of $\varepsilon = 5 \times 10^{-3}$. The black dashed, green dotted and red dash-dotted lines represent the output results with $N_\tau = 48$, 64 and 96, respectively. Figure (b) shows the results with a fixed temporal extent of $N_\tau = 96$. The black dashed, green dotted and red dash-dotted lines represent the output results with $\varepsilon = 10^{-2}$, 5×10^{-3} and 10^{-5}, respectively. In both figures, the blue solid line represents the input spectral function.

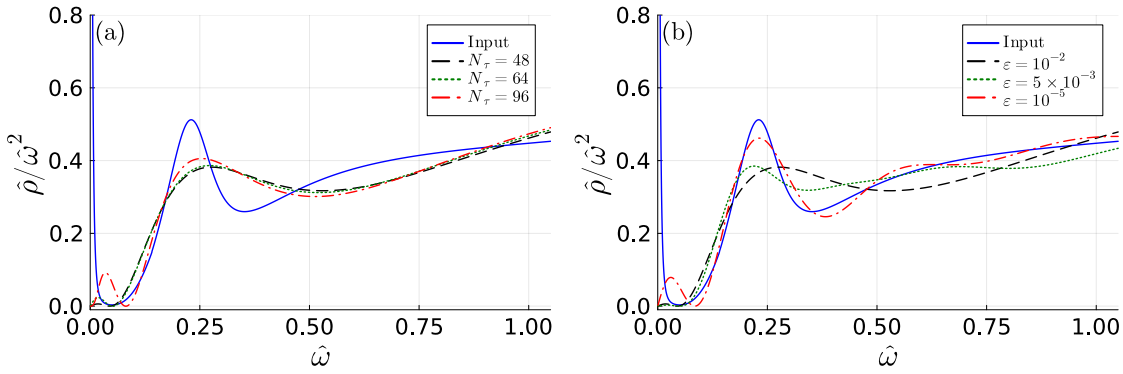

Figure 2: Same as Fig. 1 but for $T > T_c$. Figure (a) and (b) show the results with $\varepsilon = 10^{-2}$ and $N_\tau = 48$, respectively.

i.e., larger N_τ and smaller ε make the output closer to the input. Nevertheless, no transport peaks appear in the calculations for any N_τ and ε combinations.

4. Results from lattice QCD data

Next, we extracted the spectral function from actual lattice QCD data.

We used the lattice data given in ref. [14], where the correlation functions were measured with the $O(a)$-improved Wilson quark action on quenched gauge configurations generated by using the standard plaquette gauge action. The lattice spacing $a = 0.010$ fm and the corresponding a^{-1} is about 18.97 GeV. The spatial extent N_σ, the temporal extent N_τ, corresponding temperatures and the numbers of gauge configurations are summarized in table 2. We utilized meson correlation functions in the vector and the pseudoscalar channels for each temperature. We set $\hat{\tau}_0 = 4$, and used the correlation function data from $\hat{\tau}_0$ to $N_\tau/2$.

N_σ	N_τ	T/T_c	# of conf.
128	96	0.73	234
128	48	1.46	461

Table 2: The values of N_σ, N_τ, corresponding temperatures, and number of configurations.

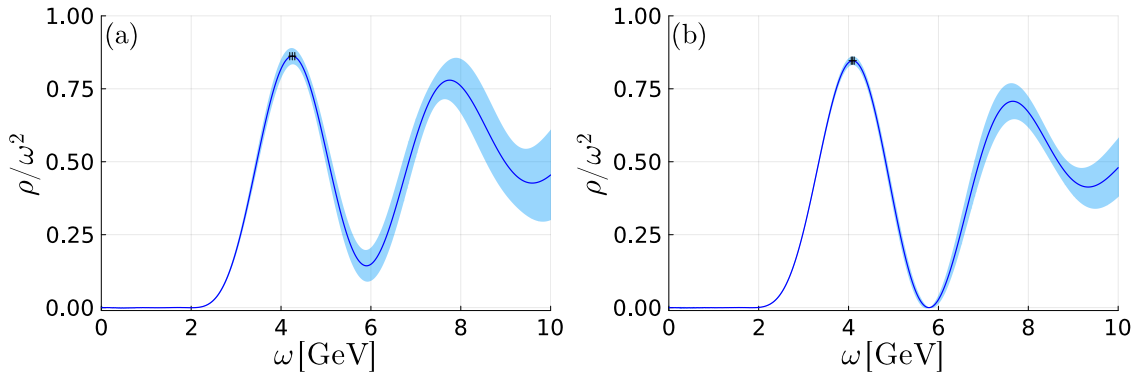

Figure 3: Spectral functions in (a) vector and (b) pseudoscalar channels extracted from actual lattice QCD data for $T < T_c$ by using sparse modeling. The blue shaded areas represent the statistical errors of the spectral functions from Jackknife analyses, the blue solid lines represent the mean values, and the black horizontal error bars represent the uncertainty of the location of the first peak for each spectral function.

Figure 3 shows our results of the spectral functions in (a) vector and (b) pseudoscalar channels for $T < T_c$. The blue shaded areas represent the statistical errors of the spectral functions from Jackknife analyses, the blue solid lines represent the mean values, and the black horizontal error bars represent the uncertainty of the location of the first peak for each spectral function. The value of the spectral function increases around 2GeV. The average value of the location of the first peak is 4.3 GeV in the vector channel and 4.1 GeV in the pseudoscalar channel, while those obtained from the maximum entropy method (MEM) are about 3.48 GeV in the vector channel and about 3.31 GeV in the pseudoscalar channel [14]. Our result is a bit larger compared to the result of the previous study.

Figure 4 shows the same as Fig. 3 but for $T > T_c$. Compared to the results for $T < T_c$, the peaks are broader and are located at higher energies. The average values of the location of the first peak are 5.7 GeV in the vector channel and 4.9 GeV in the pseudoscalar channel, while those obtained from MEM are about 4.7 GeV in the vector channel and about 4.1 GeV in the pseudoscalar channel [14]. Our results for higher temperatures are also a bit larger compared to the results of the previous study. In addition, the transport peak does not appear.

5. Summary

We applied sparse modeling for extracting a spectral function from a Euclidean-time meson correlation function. Sparse modeling is a method that solves inverse problems by considering only the sparseness of the solution we seek.

First, we tested sparse modeling with mock data of the spectral function which imitate possible charmonium spectral function for $T < T_c$ and $T > T_c$ and checked applicability of sparse modeling.

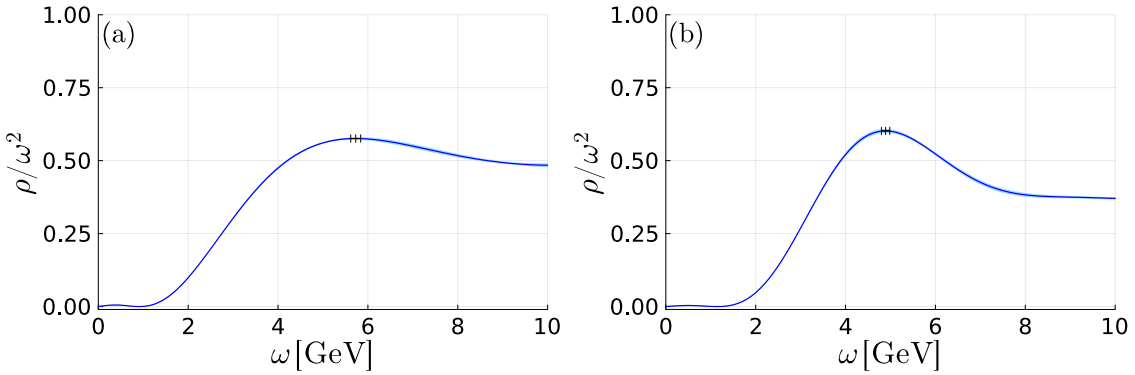

Figure 4: Same as Fig. 3 but for $T > T_c$. Figure (a) and (b) show the results in vector and pseudoscalar channels, respectively.

This test confirmed that increasing the number of data points of the correlation function and reducing the noise level of errors of the correlation function lead to output spectral functions closer to the input spectral function. Despite the inclusion of transport peaks in the input spectral function for $T > T_c$, our calculations do not yield the transport peak.

Next, we tried to extract the spectral functions from the charmonium correlation functions in vector and pseudoscalar channels for $T < T_c$ and $T > T_c$ obtained from lattice QCD. Then, we got a spectral function with a broad peak around 4 GeV in each channel for $T < T_c$, which is a bit larger compared to the results in the previous study using the maximum entropy method [14]. For $T > T_c$, compared to the results for $T < T_c$, we got a spectral function with a broader peak around 5 GeV in each channel, which is also a bit larger compared to the results from MEM. In addition, the transport peak does not appear. In order to estimate the transport peak, it may be necessary to make assumptions that extend beyond the sparse modeling, including the shape of the transport peak.

Acknowledgments

We deeply grateful to H.-T. Ding for sharing lattice data. The work of A.T. was partially supported by JSPS KAKENHI Grant Numbers 20K14479, 22H05111 and 22K03539. A.T. and H.O. were partially supported by JSPS KAKENHI Grant Number 22H05112. This work was partially supported by MEXT as "Program for Promoting Researches on the Supercomputer Fugaku" (Grant Number JPMXP1020230411, JPMXP1020230409).

References

[1] L.D. McLerran and T. Toimela, *Photon and Dilepton Emission from the Quark - Gluon Plasma: Some General Considerations*, *Phys. Rev. D* **31** (1985) 545.

[2] T. Matsui and H. Satz, *J/ψ Suppression by Quark-Gluon Plasma Formation*, *Phys. Lett. B* **178** (1986) 416.

[3] E. Braaten, R.D. Pisarski and T.-C. Yuan, *Production of Soft Dileptons in the Quark - Gluon Plasma*, *Phys. Rev. Lett.* **64** (1990) 2242.

[4] P. Petreczky and D. Teaney, *Heavy quark diffusion from the lattice*, *Phys. Rev. D* **73** (2006) 014508 [hep-ph/0507318].

[5] M. Asakawa, T. Hatsuda and Y. Nakahara, *Maximum entropy analysis of the spectral functions in lattice QCD*, *Prog. Part. Nucl. Phys.* **46** (2001) 459 [hep-lat/0011040].

[6] H.-T. Ding, O. Kaczmarek, S. Mukherjee, H. Ohno and H.T. Shu, *Stochastic reconstructions of spectral functions: Application to lattice QCD*, *Phys. Rev. D* **97** (2018) 094503 [1712.03341].

[7] B.B. Brandt, A. Francis, H.B. Meyer and D. Robaina, *Pion quasiparticle in the low-temperature phase of QCD*, *Phys. Rev. D* **92** (2015) 094510 [1506.05732].

[8] E. Itou and Y. Nagai, *Sparse modeling approach to obtaining the shear viscosity from smeared correlation functions*, *JHEP* **07** (2020) 007 [2004.02426].

[9] J. Takahashi, H. Ohno and A. Tomiya, *Sparse modeling approach to extract spectral functions with covariance of Euclidean-time correlators of lattice QCD*, *PoS* **LATTICE2023** (2024) 028 [2311.15233].

[10] H. Shinaoka, J. Otsuki, M. Ohzeki and K. Yoshimi, *Compressing Green's function using intermediate representation between imaginary-time and real-frequency domains*, *Phys. Rev. B* **96** (2017) 035147 [1702.03054].

[11] J. Otsuki, M. Ohzeki, H. Shinaoka and K. Yoshimi, *Sparse modeling approach to analytical continuation of imaginary-time quantum monte carlo data*, *Phys. Rev. E* **95** (2017) 061302 [1702.03056].

[12] J. Otsuki, M. Ohzeki, H. Shinaoka and K. Yoshimi, *Sparse modeling in quantum many-body problems*, *J. Phys. Soc. Jap.* **89** (2020) 012001 [1911.04116].

[13] S. Boyd, N. Parikh, E. Chu, B. Peleato and J. Eckstein, *Distributed optimization and statistical learning via the alternating direction method of multipliers*, *Found. Trends Mach. Learn.* **3** (2011) 1.

[14] H.T. Ding, A. Francis, O. Kaczmarek, F. Karsch, H. Satz and W. Soeldner, *Charmonium properties in hot quenched lattice QCD*, *Phys. Rev. D* **86** (2012) 014509 [1204.4945].

PoS(LATTICE2024)032